Hindawi
Journal of Chemistry
Volume 2023, Article ID 9924845, 14 pages
https://doi.org/10.1155/2023/9924845

Research Article

Antibiofilm and Anti-Quorum Sensing Potential of Safely-Synthesized Hydrated Zirconium Oxide-Coated Alginate Beads against Some Pathogenic Bacteria

Alfred Ngenge Tamfu,[1,2,3,4,5] **Yasemin Ispirli Dogaç**,[2] **Ozgur Ceylan**,[3] **Andreea Botezatu Dediu**,[4] **Selahattin Bozkurt**,[5] **and Rodica Mihaela Dinica**[4]

[1]*Department of Chemical Engineering, School of Chemical Engineering and Mineral Industries, University of Ngaoundere, Ngaoundere 454, Cameroon*
[2]*Department of Chemistry and Chemical Processing Technology, Mugla Vocational School, Mugla Sitki Kocman University, Mugla 48000, Turkey*
[3]*Food Quality Control and Analysis Program, Ula Ali Kocman Vocational School, Muğla Sitki Koçman University, Muğla, Ula 48147, Turkey*
[4]*Dunarea de Jos University, Faculty of Sciences and Environment, Department of Chemistry, Physics and Environment, 47 Domneasca Str., Galati 800008, Romania*
[5]*Vocational School of Health Services, Usak University, Usak 64200, Turkey*

Correspondence should be addressed to Alfred Ngenge Tamfu; macntamfu@yahoo.co.uk

Received 9 March 2023; Revised 3 September 2023; Accepted 28 September 2023; Published 6 October 2023

Academic Editor: Mahmood Ahmed

Water is essential to life, but access to uncontaminated water remains a global challenge. Metal oxides possess particular characteristics required for removing heavy metals, inorganic and organic pollutants from wastewater as well as inhibiting microorganisms. Zirconium oxide and alginate which are nontoxic materials were used to synthesize hydrated zirconium oxide-alginate coated materials, ZAB-1 (1.5% alginate) and ZAB-2 (2.0% alginate). FT-IR was used to characterize the functional groups while surface morphology was characterized using SEM. XRD was used to characterize the material structure of the resulting composite. Against *Chromobacterium violaceum* CV12472, minimal inhibitory concentrations (MICs) were 0.625 mg/mL for ZAB-1 and ZAB-2 while against *C. violaceum* CV026, the MIC values were 0.625 mg/mL and 1.25 mg/mL for ZAB-1 and ZAB-2, respectively. At MIC and sub-MIC concentrations, the synthesized beads inhibited the production of violacein in *C. violaceum* CV12472 and *C. violaceum* CV026, indicating that they can reduce QS-mediated virulence factors in bacteria. Antimicrobial activity was evaluated against *Staphylococcus aureus*, *Enterococcus faecalis*, *Listeria monocytogenes*, *Escherichia coli*, *Pseudomonas aeruginosa*, *Salmonella typhi*, *Candida albicans*, and *Candida tropicalis*, and MIC values ranged from 1.25 mg/mL to 10 mg/mL. Biofilm inhibition percentages were relatively high against *S. aureus*, *E. coli*, and *C. albicans*. It is observed that the increase in the alginate amount from 1.5% to 2.0% improves the antimicrobial, anti-QS, and antibiofilm effects. The alginate makes the zirconium oxide particles biocompatible and easily recoverable from water after treatment. ZAB-1 and ZAB-2 materials can therefore be sustainable materials for water treatment since it can inhibit pathogenic bacteria in water and equally satisfy environmental friendliness. The synthesized particles reduced the chances for antimicrobial resistance since they disrupted QS in bacteria and eliminated biofilms, thereby preventing biofouling of microbial communities in water. Future prospects of this study involve biofiltration, that is, the use of the synthesized composite in the development of a safe and compatible biofilter for water purification.

1. Introduction

Over 780 million people across the globe do not have access to clean and safe water, and an approximate number of about 2.5 billion people in the developing countries do not have adequate sanitation, placing them under a high risk of waterborne diseases [1, 2]. Waterborne diseases which are caused by various pathogens usually transmitted through water constitutes a major health challenge, resulting in mortalities and morbidities and some of them are directly resulting from deterioration of the environment and pollution [3]. Although many efforts are being made to ensure safe water, outbreaks of waterborne infections continue to appear throughout the globe. More than 400 microorganisms cause waterborne diseases and have different origins and modes of transmission but more than 95% of these waterborne diseases can be prevented. However, some factors such as lack of resources, emerging resistant pathogens, and chemical contaminants make it difficult [4]. Some of the bacteria in water usually evolve into resistant strains that are able to survive the effects of disinfectants, detergents, and antibiotics, making biological treatment of water difficult to achieve except by targeting their quorum sensing network, thus demanding the search for new alternative water treatments. Quorum sensing (QS) involves a cell-cell communication system in bacterial life processes involving secretion, detection, and response to small signalling molecules known as autoinducers (AIs) [5, 6]. QS controls virulence factors in bacteria such as biofilm formation, violacein production, and motilities [7]. Most of the microbial resistance mechanisms and virulence include antibiotic efflux pumps, pathogenic gene expression, swarming motility, the production of toxins, and formation of biofilm [8]. It is therefore a suitable strategy to search for quorum-quenching materials which can prevent microbial resistance and use them against drug-resistant pathogens [9]. However, water is usually contaminated by both biological contaminants and chemical substances. Metal oxides with or without polymers have demonstrated important properties such as antibacterial, adsorption, magnetic properties, large surface area, and surface mobility [10]. Such polymer-metal oxide nanocomposites are more potent in water treatment since they possess high photodegradation activity toward pollutants under simulated visible light [10]. Polymer nanoparticles are highly used in eliminating pollutants from water because of their tuneable surface chemistry, large surface area, pore size distribution, and perfect mechanical rigidity [11].

As a result of various industrial applications, metals (such as arsenic, cadmium, chromium, mercury, nickel, and lead) can leak into wastewater and unfortunately, pollute the waters and negatively affect the aquatic ecosystem [12–14]. In addition, exposure to such metal residues causes some health problems such as liver damage, lung congestion, and shortness of breath [15]. Physical and chemical methods such as chemical precipitation, electrolysis, ion exchange, membrane filtration, solvent extraction, reverse osmosis, and liquid extraction are used to remove such metals from wastewater [16–19]. Removal of metals using these methods is costly [16, 20, 21]. Therefore, using adsorption methods to remove metals is very advantageous in terms of simplicity and cost reduction [14, 19, 21–30]. In the literature, cerium, iron, manganese, aluminium, titanium, and zirconium-based oxides/hydroxides, and nanometal oxides/hydroxides have been extensively studied for metal removal from wastewater [14, 31–38].

Among the metallic materials used in water purification, zirconium-based particles are of great interest [14, 27, 39–41]. The possible rich hydroxyl groups on the zirconium-based particles are responsible for metal removal via ligand or ion exchange [42]. Zirconium-based materials are water-insoluble, nontoxic, and stable [43]. However, their use alone can cause the release of particles into the water, which can potentially harm native flora and fauna. To solve this, these adsorbents are made into composites with supportive biomaterials. Forming composites of Zr-based particles with supports such as alginate beads [44–46], chitosan beads [46–48], polystyrene anion exchanger [46, 49], and carbon nanotubes has been reported to be highly effective in preventing the release of this adsorbent into the environment [46, 50, 51]. Of these, alginate has a strong affinity for metal ions. Metal ions (positively charged) are electrostatically attracted to negatively charged carboxyl groups in calcium alginate. The synthesis of various adsorbents made up of alginate beads, cross-linked with calcium ions is usually an environmentally friendly method [28, 46, 52]. These composites can be used to remove both cationic and anionic contaminants from wastewater. Generally, hydrothermal [42], precipitation [27], and sol-gel methods [39] are used to synthesize Zr-based composite. The filtration-steam hydrolysis method is a simple way of coating the polymer with the metal oxides [53]. The morphology and thickness of this coating help in increasing the specific surface area and also increasing adsorption. It is known that metal alkoxide can be reduced to alcohol (A) and hydrated metal oxide after a filtration-steam hydrolysis reaction. It has been reported that the hydrated zirconium oxide ($ZrO(H_2O)$) formed from such a process is composed of many hydrated polymeric species such as ZrAO, HAOAH, and ZrAOH [54, 55].

The adsorption capacities of Zr-based materials have been demonstrated in many studies, especially on the removal of metal ions from wastewater, as described above. Based on our knowledge, there is no study in the literature that determines the antimicrobial properties of zirconium oxide materials especially for waterborne pathogens. Therefore, the aim of the present study is to synthesize hydrated zirconium oxide-alginate beads and determine their effects on virulence factors of some major waterborne pathogens.

2. Materials and Methods

2.1. Synthesis of Alginate Beads. The alginate beads were synthesized by the sol-gel templating method, as described elsewhere [14]. Sodium alginate was dissolved in deionized water to prepare alginate solutions with different percentages, that is, 1.5 wt % (alginate solution 1) or 2.0 wt %

(alginate solution 2). Each of the alginate solutions was added dropwise to a 2% (w/v) calcium chloride solution in order to cross-link the alginate with the Ca^{2+} ions to form alginate beads. The alginate beads were incubated in the calcium chloride solution overnight. Then, the beads were washed with deionized water several times to give AB-1 beads from alginate solution 1 (1.5 wt %) and AB-2 beads from alginate solution 2 (2.0 wt %).

2.2. Preparation of Hydrated Zirconium Oxide-Coated Alginate Beads. Hydrated zirconium oxide-coated alginate beads were prepared by a filtration-steam hydrolysis method described previously [14]. 150 beads of alginate (AB-1 and AB-2) and 5 mL of zirconium n-propoxide were dispersed in 50 mL of absolute ethanol by sonication for 1 hour. The mixture was filtered under vacuum through a polytetrafluoroethylene membrane. Then, water vapor at 75°C was passed through the beads for 2 hours to induce the formation of hydrated zirconium oxide on the surface of the beads. After this procedure, the beads were washed several times with distilled water/ethanol (50 : 50) solution. The hydrated zirconium oxide-coated alginate beads were dried at 100°C overnight. They were denoted ZAB-1 and ZAB-2 obtained from AB-1 (1.5 wt % alginate) and AB-2 (2.0 wt % alginate), respectively. In addition, hydrated zirconium oxide ($ZrO(H_2O)$) was synthesized by the hydrolysis method to be used as a control group in characterization analyses. Again, 5 mL of zirconium n-propoxide was dissolved in 50 mL of absolute ethanol, and the mixture was sonicated for 1 hour. The product was washed several times with distilled water/ethanol (50 : 50) solution. The hydrated zirconium oxide was dried at 100°C overnight. The schematic representation of the synthesis is given in Figure 1.

2.3. Characterization of Hydrated Zirconium Oxide-Coated Alginate Beads. Surface groups and chemical structure of raw hydrated zirconium oxide, raw alginate, and hydrated zirconium oxide-coated alginate beads were analyzed using Fourier transform infrared (FT-IR) spectroscopy. The surface morphology hydrated zirconium oxide-coated alginate beads was analyzed by scanning electron microscopy (SEM) a JEOL JSM 7600 F model equipment. The X-ray diffraction (XRD) analysis was performed using a Rigaku Miniflex Desktop XRD device with a Cu Kα radiation ($\lambda = 1.5406$ Å) source. The sample was scanned in continuous mode with a step size of 0.01° s, from 5 to 90° (2θ), with a scanning rate of 10°/min produced at 40 kV and 30 mA.

2.4. Microbial Strains. The following waterborne pathogens were used in the assays: *Staphylococcus aureus* ATCC 25923, *Enterococcus faecalis* ATCC 29212, *Listeria monocytogenes* ATCC 7644, *Escherichia coli* ATCC 25922, *Pseudomonas aeruginosa* ATCC 27853, *Salmonella* Typhi ATCC 14028, *Candida albicans* ATCC 10239, *Candida tropicalis* ATCC 13803, *Chromobacterium violaceum* CV12472, *Chromobacterium violaceum* CV026, and *Pseudomonas aeruginosa* PA01. The Gram-positive bacteria *Staphylococcus aureus, Listeria monocytogenes*, and *Enterococcus faecalis* have been described to infect humans through the consumption of contaminated water or seafood are therefore part of water pathogens [3]. The Gram-negative bacteria involved in this study are *Escherichia coli*, *Pseudomonas aeruginosa*, and *Salmonella* Typhi which have been described as pathogens involved in waterborne diseases [56]. Candida species including *Candida albicans* and *Candida tropicalis* together with other opportunistic yeasts have been detected in polluted waters [57]. *Chromobacterium violaceum* is an opportunistic Gram-negative bacillus that inhabit soil and water environments especially in tropical and subtropical regions [58].

2.5. Antimicrobial Activity Assay by Minimal Inhibitory Concentration (MIC) Determination. The MIC of each sample was evaluated using the broth microdilution method as described [59]. MIC is the lowest concentration that inhibited visible growth and was determined using a spectrophotometer [9]. Mueller–Hinton broth (MHB) was used with microbial density of 5×10^5 colony-forming units (CFU)/mL. 10 μL of microbial solution were inoculated into 200 μL wells containing MHB (170 μL) and test sample (20 μL) with different concentrations samples (10, 5, 2.5, 1.25, 0.625, and 0.312 mg/mL). The plates were read at 600 nm using a multiscan Go microplate reader (Thermo Fischer Scientific, Waltham, MA, USA) after incubation for 24 h at 37°C.

2.6. Evaluation of Percentage Inhibition of Biofilm Using the Crystal Violet Staining Method. The antibiofilm activity at MIC and sub-MIC concentrations (1, 1/2, 1/4, and 1/8 MIC) of ZAB-1 and ZAB-2 were measured, as described previously [60, 61]. Briefly, tryptose-soy broth (TSB) containing 0.25% glucose was used and 1% (v/v) overnight microbial cultures were added to 200 μL wells with or without ZAB-1 and ZAB-2 at their MIC and sub-MIC. The wells with only media and microbial cells served as control. After 48 hours incubation, planktonic bacteria were removed, and the wells were stained with 0.1% crystal violet in distilled water for 10 minutes. After removing the crystal violet, 200 μL of ethanol or 200 μL of 33% glacial acetic acid were filled into the wells, and 125 μL from each well was pipetted into a sterile tube and made up to 1 mL volume with distilled water. The optical density was read at 550 nm (Thermo Scientific Multiskan FC, Vantaa, Finland), and the percentage inhibition of biofilm calculated as follows:

$$\text{Biofilm inhibition } (\%) = \frac{\text{OD550}_{\text{Control}} - \text{OD550}_{\text{Sample}}}{\text{OD550}_{\text{Control}}} \text{ x } 100. \quad (1)$$

2.7. Quorum Sensing Inhibition (QSI) Activity of Samples on C. violaceum CV026. Inhibition of quorum sensing (QS) was performed, as described previously [62, 63]. Briefly, 100 μL of overnight CV026 culture was added to 5 mL of warm molten soft agar (200 mL H2O, 1.3 g agar, 1.0 g NaCl,

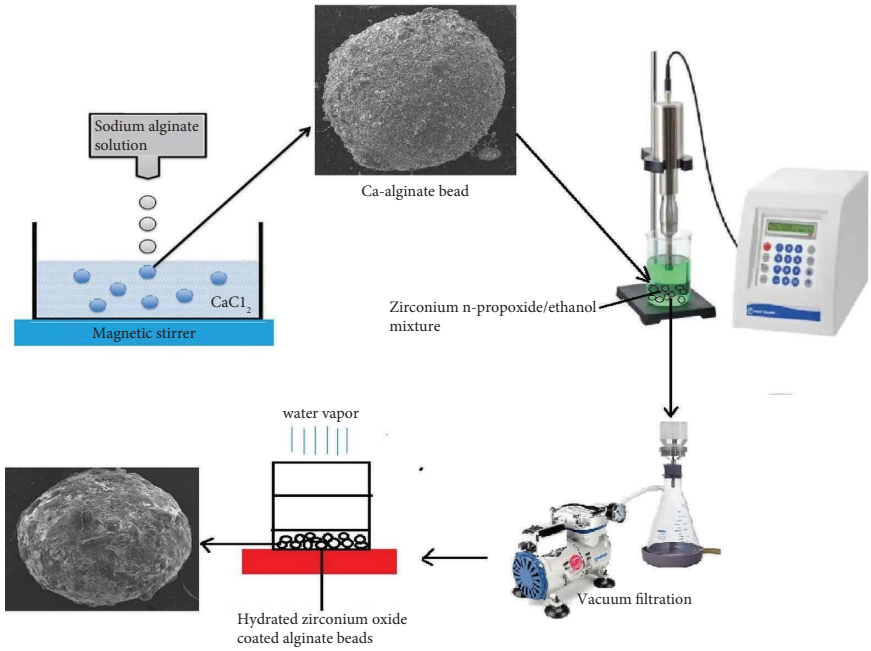

Figure 1: Scheme for the synthesis of hydrated zirconium oxide-coated alginate beads.

2.0 g tryptone) together with 20 μL of exogenous C6HSL (100 μg/mL) acylhomoserine lactone (AHL). The mixture was stirred and poured over LBA agar plates as an overlay. 5 mm diameter wells were made on the plate surfaces into which 50 μL of sterilized ZAB-1 and ZAB-2 were added, and the plates incubated at 30°C for 3 days. After this, a cream-coloured halo around each well indicated QSI, and the diameters were recorded in millimetres. Each experiment was done in triplicate.

2.8. Violacein Inhibition of Samples of C. violacium CV12472. ZAB-1 and ZAB-2 were evaluated for qualitative inhibition of violacein pigment to find out their QSI potential using *C. violaceum* ATCC 12472 [64, 65]. 10 μL of C. violaceum overnight cultures, adjusted to 0.4 OD at 600 nm, were added to a 200 μL well containing LB broth in the presence and absence of 20 μL MIC and sub-MICs of samples. *C. violaceum* ATCC 12472 in LB broth without samples was used as a control. These plates were incubated for 24 hours at 30°C, and the reduction in violacein pigment production was measured through absorbances at 585 nm. The violacein inhibition percentages were calculated using the following formula:

$$\text{Violacein inhibition (\%)} = \frac{\text{OD 585 control} - \text{OD585 sample}}{\text{OD 585 control}} \text{x100.} \quad (2)$$

2.9. Swarming Motility Inhibition in P. aeruginosa PA01. Swarming motility inhibition was performed, as described elsewhere [66, 67]. Briefly, *P. aeruginosa* PA01 overnight cultures were inoculated at the center of swarming plates (0.5% agar, 1% peptone, 0.5% D-glucose, and 0.5% NaCl) containing concentrations of 50, 75, and 100 µg/mL of ZAB-1 and ZAB-2. The plates without ZAB-1 and ZAB-2 served as controls. Plates were incubated at 37°C in an upright position for 18 h. The area covered by bacterial growth or swarming migration fronts was recorded, and the percentage inhibition of the swarming movement was calculated.

2.10. Statistical Analysis. Each experiment was repeated three times, and the results are expressed as means ± standard error of the mean. The Student's test was used to determine the significant differences between various means, and the values for $p < 0.05$ were regarded as significant.

3. Results and Discussion

3.1. Characterization of Hydrated Zirconium Oxide-Coated Alginate Beads. The encapsulation of hydrated zirconium oxide into the alginate beads was verified by Fourier transform infrared spectroscopy (FT-IR). The FT-IR spectra of the raw hydrated zirconium oxide, raw sodium alginate, and hydrated zirconium oxide-coated alginate beads are shown in Figure 2. In the FT-IR of raw hydrated zirconium oxide (Figure 2), the bands with absorption maxima at approximately 1630 cm^{-1} and 3450 cm^{-1} were attributed to the bending and stretching vibrations of hydroxyl groups,

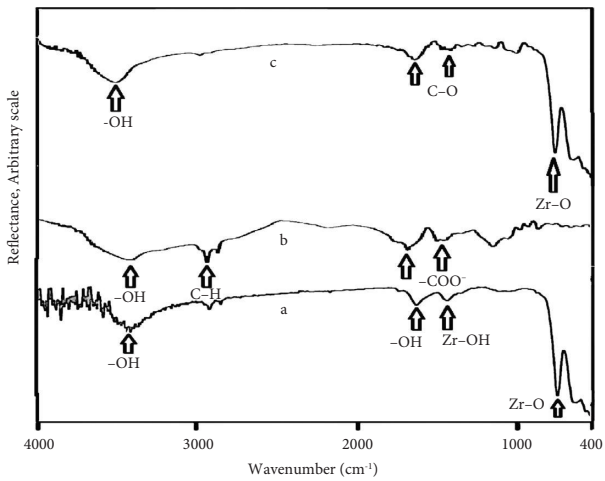

Figure 2: FT-IR spectra of raw hydrated zirconium oxide (a), raw sodium alginate (b), and hydrated zirconium oxide-coated alginate beads (c).

which are linked to the zirconium oxide. The band around 650 cm^{-1} corresponded to the Zr-O stretching vibration. Also, the band at approximately 1440 cm^{-1} was attributed to the bending vibration of Zr-OH. The FT-IR spectra of sodium alginate (Figure 2) indicated important bands attributable to the hydroxyl and carboxylic functional groups. Stretching vibrations of hydroxyl groups of alginate were seen in the range of 3000–3600 cm^{-1}, as a broad band. Stretching vibrations of aliphatic C-H bonds appeared at 2900–2850 cm^{-1}. The observed bands at 1650 and 1450 cm^{-1} were attributed to the asymmetric and the symmetric vibrations of carboxylate ion, respectively. The bands in the spectra after cross-linking of alginate with calcium ions followed by coating with hydrated zirconium oxide (Figure 2) enabled the characterization of the alginate structure coated with hydrated zirconium oxide. The bands observed at 1100 and 930 cm^{-1} correspond to the C-O stretching vibration of the pyranosyl ring and the C-O stretching with contributions from C-C-H and C-O-H deformation. In addition, the band around 650 cm^{-1} can be attributed to the Zr-O stretching vibration. So, this shows that the synthesis and encapsulating processes were successfully achieved. Notably on the FT-IR, the bending and stretching vibrations of hydroxyl groups linked to the zirconium oxide were at 1630 cm^{-1} and 3450 cm^{-1}, and the Zr-OH bending vibration was at approximately 1440 cm^{-1} [68, 69]. Hydrated zirconium oxide-coated alginate beads exhibited stretching vibrations of hydroxyl groups smaller than those for sodium alginate since the hydroxyl and carboxylate groups of alginate and the Ca^{2+} are chelated [70].

SEM analysis was performed to determine the morphology of the alginate bead without hydrated zirconium oxide in comparison with that of hydrated zirconium oxide-coated alginate beads, and SEM photographs are given in Figure 3. In both types of beads, the difference in roughness of the surfaces is clearly visible. In Figure 3, it is clear that after the zirconium oxide coating, the roughness on the surface of the beads increases accordingly and appreciably upon the addition of hydrated zirconium oxide in the surface area of the beads.

The XRD pattern for the synthesized hydrated zirconia-alginate beads with 2% alginate (ZAB-2) is given in Figure 4. The intensity and sharpness of the dominant diffraction peaks can reflect the purity of the synthesized hydrated zirconium oxide-alginate beads. The significant diffraction peaks that are comparable to the reported data for monoclinic ZrO_2 suggest high crystallinity as well. The strongest diffraction peak at 28.1° observed here has been described as the characteristic (111) plane of the monoclinic zirconia phase. The prominent peak at around 30°, usually attributed to the characteristic spacing (101) for tetragonal zirconia is absent on the XRD patterns for ZAB-2. The absence of the most important peak for tetragonal zirconia which occurs at 30° and corresponds to the spacing (111) for tetragonal zirconia, indicates an almost monoclinic nature. All the observed reflection peaks are referable and matched with the JCPDS (01-089-9066) for a dominant monoclinic phase of zirconia. The characteristic peaks at 2θ angles 28.1, 35.6, 39.8, 45.6, 49.6, 54.2, 55.3, 57.0, 60.2, 68.1, 74.0, and 76.5 have been described as characteristic for the existence of monoclinic phase of ZrO_2. However, there were some shifts in peak positions at some points, which indicates some changes in the structure due to the added alginate. The XRD patterns for the ZAB-2 sample indicate a few additional peaks with low intensities which could be ascribable to a trace of the tetragonal phase (340, 350 and 60.20) and calcium alginate (20° and 28.5°) matrix. The peaks at 2θ 34°, 35°, and 60.2° were described as characteristic peaks of the tetragonal phase of zirconia while those at 20.06° and 28.96° are known to be calcium alginate peaks. The most important and majority of peaks in ZAB-2 are comparable to those in a reported study which were attributed to the monoclinic ZrO_2 phase in a sample containing both monoclinic and tetragonal ZrO_2 phases, and it was concluded that the monoclinic phase was greater than the tetragonal phase in terms of content. Summarily, on the XRD patterns of ZAB-2, there was the presence of the major diffraction maxima attributable to zirconium dioxide monoclinic phase ascribable to the spacings (111), (002), (112), (202), (013), (311), (023), and (114) which are thoroughly described in the literature. The FT-IR and XRD data were in conformity with the characteristic information reported for ZrO_2. The characteristic XRD diffraction peak of the monoclinic zirconia phase appeared at 28.1° and there was an absence of a tetragonal zirconia diffraction peak at 30°, suggesting an almost monoclinic nature [71, 72]. Other prominent monoclinic zirconia peaks occurred at 2θ angles 28.1, 35.6, 39.8, 45.6, 49.6, 54.2, 55.3, 57.0, 60.2, 68.1, 74.0, and 76.5 in conformity with reported data [73–75]. The peaks at 2θ 20.06° and 28.96° are attributable to calcium alginate [75, 76]. Most of the important peaks of ZAB-1 and ZAB-2 are in agreement with those of ZrO_2 with the dominant monoclinic phase [77–79].

Biopolymer-metal oxide hybrids such as the ZAB-1 and ZAB-2 synthesized in this study enable chemists to combine the high-tech properties of metal oxides with those of biopolymers and such materials have biological activities

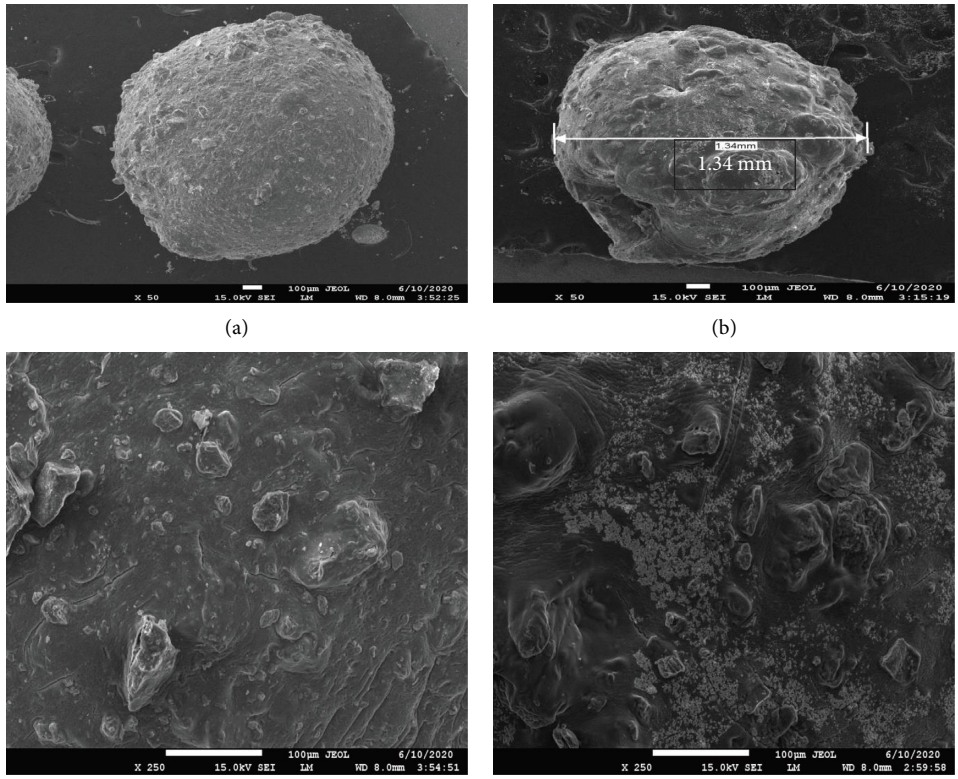

Figure 3: SEM micrographs of alginate bead without hydrated zirconium oxide coating ((a) X100 and (c) X250) and hydrated zirconium oxide-coated alginate beads ((b) X100 and (d) X250).

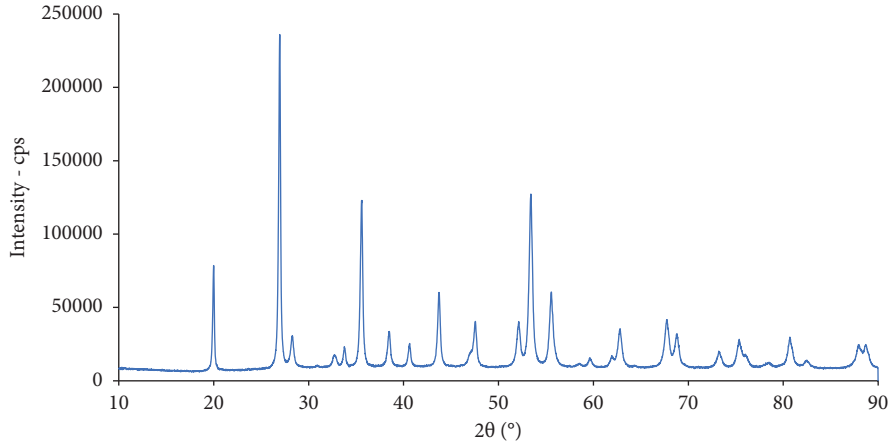

Figure 4: XRD patterns for ZAB-2 (hydrated zirconia-alginate beads with 2% alginate).

including antimicrobial properties [80, 81]. They are usually prepared by dispersing metal oxides into commercially available polymers, as in this study or by incorporating metal oxides during the polymerization process [82]. The encapsulation of the zirconium oxide particles into a natural biopolymer such as alginate makes them more compatible with the environment and living systems and also enables them not to contaminate or leak into the environment while maintaining their properties. Dispersing metal oxides in a biopolymer also improves catalytic, surface, and magnetic properties as well as their weights which facilitates their sedimentation and recovery from the aqueous medium during the water purification process [83]. This means that the synthesized hydrated zirconium oxide-alginate-coated beads (ZAB-1 and ZAB-2) possess suitable properties for wastewater treatment. This can be attributed to its absorption properties and antiseptic nature. The added advantage is that ZAB-1 and ZAB-2 satisfy environmental exigencies due to their biocompatibility and ease of recovery after usage.

3.2. Antimicrobial and Antibiofilm Activities. The antimicrobial activity of the synthesized beads was determined against three Gram-positive bacteria, three Gram-negative bacteria, and two fungi (Table 1). The MIC values of both ZAB-1 and ZAB-2 were 1.25 mg/mL against *E. faecalis* and 5 mg/mL against *L. monocytogenes*. Against *S. aureus*, the MIC values were 2.5 mg/mL and 1.25 mg/mL for ZAB-1 and ZAB-2, respectively. The MIC values of ZAB-1 and ZAB-2 were 10 mg/mL against *P. aeruginosa* and 2.5 mg/mL against *S.* Typhi. Against *E. coli*, MIC values were 10 mg/mL and 5 mg/mL for ZAB-1 and ZAB-2, respectively. For the yeast cells, MIC values of ZAB-1 and ZAB-2 were 2.5 mg/mL against *C. albicans*. The MIC values of ZAB-1 and ZAB-2 against *C. tropicalis* were 5 mg/mL and 2.5 mg/mL, respectively. The antimicrobial activity was almost the same for both beads except against *S. aureus*, *E. coli*, and *C. tropicalis*, against which ZAB-2 was more active than ZAB-1.

Most antimicrobial substances have limited efficacy because they are able to eliminate or inhibit planktonic bacterial communities but are often challenged by biofilm bacterial communities, which are difficult to treat. Biofilms consist of a protective polymeric matrix developed by pathogenic yeasts, Gram-positive and Gram-negative bacteria, and helps them to adapt to environmental stress, antibiotics, starvation, and host immune system [84]. The ability of the synthesized beads (ZAB-1 and ZAB-2) to inhibit biofilms was evaluated at MIC and sub-MIC concentrations and reported in Table 2. ZAB-1 inhibited the biofilm of *S. aureus* with percentage inhibition varying from 26.47 ± 0.42% at MIC to 04.83 ± 0.11% at MIC/4. The biofilm inhibition percentage of ZAB-2 against *S. aureus* varied from 74.22 ± 2.24% at MIC to 08.70 ± 0.63% at MIC/8. Against *E. faecalis*, biofilm percentage inhibition varied from 14.56 ± 0.13% at MIC to 5.06 ± 0.07% at MIC/2 for ZAB-1 and from 22.91 ± 1.27% at MIC to 12.65 ± 0.55% at MIC/2 for ZAB-2. This variation was similar to that observed against another Gram-positive bacteria *L. monocytogenes*. ZAB-2 showed slightly higher antibiofilm activity than ZAB-1 against Gram-positive bacteria.

For the Gram-negative bacteria, inhibition of *E. coli* biofilm varied from 32.41 ± 0.65% at MIC to 16.98 ± 0.75% at MIC/4 for ZAB-1 and from 55.26 ± 2.02% at MIC to 14.13 ± 0.21% at MIC/2 for ZAB-2. Against *P. aeruginosa*, biofilms were inhibited only at MIC and were 13.15 ± 0.89% and 13.78 ± 0.39% for ZAB-1 and ZAB-2, respectively. It was observed that biofilm inhibition was higher against *E. coli* and *P. aeruginosa* for ZAB-2 than ZAB-1. Against *S.* Typhi, antibiofilm activity was found to be 13.9 ± 0.83% at MIC for ZAB-1 and for ZAB-2, 14.50 ± 0.28% at MIC, and 6.80 ± 0.07% at MIC/2. The beads inhibited fungal biofilms almost to the same extent. Inhibition of *C. albicans* biofilm varied from 32.46 ± 0.32% (MIC) to 09.22 ± 0.5% (MIC/2) for ZAB-1 and from 35.22 ± 0.15% (MIC) to 10.25 ± 0.35% (MIC/2) for ZAB-2. Antibiofilm activity against *C. tropicalis* varied from 38.38 ± 0.61% (MIC) to 09.21 ± 0.35% (MIC/4) for ZAB-1 and from 43.33 ± 0.64% (MIC) to 11.35 ± 0.42% (MIC/4) for ZAB-2. The fact that the hydrated zirconium oxide-coated alginate beads could act as antimicrobial substances and inhibit biofilms is critically important.

Table 1: Antimicrobial activity (MIC in mg/mL) of test samples.

Microorganisms	Sample codes	
	ZAB-1	ZAB-2
S. aureus	2.5	1.25
E. faecalis	1.25	1.25
L. monocytogenes	5	5
E. coli	10	5
P. aeruginosa	10	10
S. Typhi	2.5	2.5
C. albicans	2.5	2.5
C. tropicalis	5	2.5

Table 2: Antibiofilm activity (inhibition %) results of test samples.

Microorganisms	Concentration	ZAB-1	ZAB-2
S. aureus	MIC	26.47 ± 0.42	74.22 ± 2.24
	MIC/2	11.26 ± 0.25	41.25 ± 1.86
	MIC/4	04.83 ± 0.11	23.44 ± 0.90
	MIC/8	—	08.70 ± 0.63
E. faecalis	MIC	14.56 ± 0.13	22.91 ± 1.27
	MIC/2	5.06 ± 0.07	12.65 ± 0.55
	MIC/4	—	—
	MIC/8	—	—
L. monocytogenes	MIC	25.00 ± 1.10	28.64 ± 1.21
	MIC/2	10.14 ± 0.53	11.80 ± 0.1
	MIC/4	—	—
	MIC/8	—	—
E. coli	MIC	32.41 ± 0.65	55.26 ± 2.02
	MIC/2	16.98 ± 0.75	23.08 ± 0.61
	MIC/4	—	14.13 ± 0.21
	MIC/8	—	—
P. aeruginosa	MIC	13.15 ± 0.89	13.78 ± 0.39
	MIC/2	—	—
	MIC/4	—	—
	MIC/8	—	—
S. Typhi	MIC	13.9 ± 0.83	14.50 ± 0.28
	MIC/2	—	6.80 ± 0.07
	MIC/4	—	—
	MIC/8	—	—
C. albicans	MIC	32.46 ± 0.32	35.22 ± 0.15
	MIC/2	09.22 ± 0.5	10.25 ± 0.35
	MIC/4	—	—
	MIC/8	—	—
C. tropicalis	MIC	38.38 ± 0.61	43.33 ± 0.64
	MIC/2	20.53 ± 0.14	27.50 ± 0.35
	MIC/4	09.21 ± 0.35	11.35 ± 0.42
	MIC/8	—	—

—: no inhibition.

The antimicrobial effects of zirconium oxide material are demonstrated in this study while the absorption capacities have been reported in other reports. Metal oxides possess suitable properties for the removal of heavy metals, inorganic pollutants, and organic pollutants from wastewater and also killing microorganisms [85]. Wastewater is the major cause of waterborne diseases such as deadly cholera and typhoid and usually contains bacteria and viruses as well

as toxic chemical substances and heavy metals. Metal oxides such as TiO_2, ZnO, Ag_2O, and CuO in addition to polymer/metal oxide-based materials can use their photocatalytic degradation, adsorption, and antimicrobial activities as a multifaceted strategy to treat waste water [85, 86]. Most treatments for water are focused on removal of dirty particles and toxic chemicals while little attention is paid to health-threatening microorganisms [87–89]. The inhibitory effects against microorganisms by ZAB-1 and ZAB-2 offer additional relevance as a suitable biocide for water treatment. The alginate beads contribute in improving antimicrobial activity and also in avoiding the dispersion of the metal oxide particles in water after treatment. Polymer-metal oxide nanocomposites are efficient disinfectants for water, and it was suggested that oxides of Ag, Ti, and Zn are able to inhibit various waterborne disease microbes owing to their charge capacity [10, 90]. To the best of our knowledge, this is the first report of the biocidal effects of zirconium oxide-alginate beads. It can be observed that the antimicrobial activity in some cases increased with the increase in the percentage composition of alginate from 1.5% to 2.0%. This was the case with *S. aureus*, *E. coli*, and *C. tropicalis*. In some bacteria, the amount of alginate did not influence the antimicrobial activity as seen in the cases of *E. faecalis*, *L. monocytogenes*, *P. aeruginosa*, *S.* Typhi, and *C. albicans*. Alginate is amongst the nondigestible polysaccharides with antimicrobial and antibiofilm potential and can be used as adjuvants in combined antimicrobial therapies. In one study, alginate (2–16%) exhibited significant inhibition of microbial growth and could also prevent biofilm formation [91]. This could justify the fact that ZAB-2 (2% alginate) showed higher biofilm inhibition and antimicrobial activity on some test pathogens than ZAB-1 (1.5% alginate). Biofilms are a major cause of microbial resistance, and they can be established in almost any environment including water. Biofilms can be formed between one or more bacterial colonies and mixed biofilms are more resistant and can withstand common antibiotics, a lack of nutrients, and environmental stress. Many biopolymers such as chitosan, cellulose, starch, gelatine, collagen, alginates, pectin, hyaluronic acid, and fibrin are usually combined with antimicrobial substances to obtain biodegradable and biocompatible composites for antimicrobial applications [92].

3.3. Violacein Inhibition against C. violaceum CV12472 and Anti-Quorum Sensing against C. violaceum CV026. *Chromobacterium violaceum* CV12472 is a bacterium that produces a violet-coloured pigment known as violacein while growing under normal conditions. This pigment can be easily measured, and its production represents a quorum sensing process in bacteria. Violacein synthesis in this Gram-negative bacterium is a QS-regulated expression influenced by acylhomoserine lactones (AHLs) [93]. The MICs of the test samples on *C. violaceum* CV12472 were determined, and their violacein inhibition percentages were evaluated at MIC and sub-MIC concentrations and reported in Table 3. The MIC values were found to be 0.625 mg/mL on *C. violaceum* 12472 for both samples, ZAB-1 and ZAB-2. At MIC concentration, both samples had violacein inhibitions of 100% (determined from the optical density spectrophotometrically), but at MIC/2, ZAB-2 had violacein inhibition of 100% while ZAB-1 had 78.2 ± 1.6%. This activity reduced in a concentration-dependent manner, and at MIC/16, the inhibition percentages were 10.6 ± 0.3% and 25.1 ± 0.4% for ZAB-1 and ZAB-2, respectively, while at MIC/32, only ZAB-2 could inhibit violacein production with percentage inhibition of 9.3 ± 0.1%. The results indicate that ZAB-2 (2.0% wt alginate) possesses a slightly greater activity than ZAB-1 (1.5% wt alginate).

C. violaceum CV026 is a biosensor and wild mutant strain, which is either incapable of producing autoinducers such as AHL or deficient in AHL synthase and therefore requires an exogenous source of AHL to enable it produce violacein. For this reason, it serves as an important tool for studying QS mechanisms involving QS inhibitors of the signal molecules [94, 95]. The MIC values of the samples on *C. violaceum* CV026 were determined and reported in Table 4 alongside quorum sensing inhibition zone diameters against *C. violaceum* CV026 in the midst of an externally supplied AHL. The MIC values against *C. violaceum* CV026 were found to be 0.625 mg/mL and 1.25 mg/mL for ZAB-1 and ZAB-2, respectively. The anti-QS zone diameters were 13.0 ± 0.5 mm (ZAB-1) and 13.5 ± 0.8 mm (ZAB-2) at MIC and 9.6 ± 0.1 mm (ZAB-1) and 10.0 ± 0.5 mm (ZAB-2) at MIC/2. At MIC/4, only ZAB-2 had an inhibition zone of 7.5 ± 0.3 mm while none of the samples inhibited QS against *C. violaceum* CV026 at MIC/8. There were no significant differences between the values of the anti-QS zones of both ZAB-1 and ZAB-2.

To effectively deal with resistant biofilm colonies, it is necessary to target quorum sensing networks since quorum sensing controls and regulates biofilm formation. Quorum sensing (QS) and biofilm disruption by the synthesized hydrated zirconium oxide-alginate beads provide an efficient strategy to prevent microbial infections and resistance. QS involves cell-to-cell communication in bacteria through the production and reception of small signal molecules called autoinducers which allow the bacteria to monitor their environment, population density, and control the expression of virulence genes and pathogenesis [96, 97]. *Chromobacterium violaceum* is a bacterium that occurs in various environments mostly in tropical regions, usually contaminates water and soils and can cause some rare and often fatal diseases. This bacterium is used as a model for quorum sensing (QS) inhibition. *Shewanella spp.*, *Aeromonas spp.*, *Vibrio spp.*, and *Chromobacterium violaceum* are the four Gram-negative oxidase-positive bacteria which are usually associated with waterborne infections in tropical regions [98, 99]. It is therefore of great importance, as both ZAB-1 and ZAB-2 inhibited violacein production (QS) against the model organisms *C. violaceum* CV12472 and *C. violaceum* CV026. This bacterium produces a violet violacein pigment, a protective signal molecule which is easily measurable and represents a quorum sensing process [100]. *C. violaceum* CV12472 has intrinsic secretion of AHL and produces violacein when growing normally, and a decrease in this

Table 3: Violacein inhibition in *C. violaceum* CV12472 by the samples.

Sample code	MIC (mg/mL)	Violacein inhibition (%)					
		MIC	MIC/2	MIC/4	MIC/8	MIC/16	MIC/32
ZAB-1	0.625	100 ± 0.00	78.2 ± 1.6	51.5 ± 0.2	27.9 ± 0.5	10.6 ± 0.3	—*
ZAB-2	0.625	100 ± 0.00	100 ± 0.00	65.1 ± 1.2	43.7 ± 0.7	25.1 ± 0.4	9.3 ± 0.1

—*: no inhibition.

Table 4: Quorum sensing inhibition zones in *C. violaceum* CV026 by samples.

Sample code	Anti-quorum sensing inhibition zones (mm)				
	MIC (mg/mL)	MIC	MIC/2	MIC/4	MIC/8
ZAB-1	0.625	13.0 ± 0.5	9.6 ± 0.1	—	—
ZAB-2	1.25	13.5 ± 0.8	10.0 ± 0.5	7.5 ± 0.3	—

—: no activity.

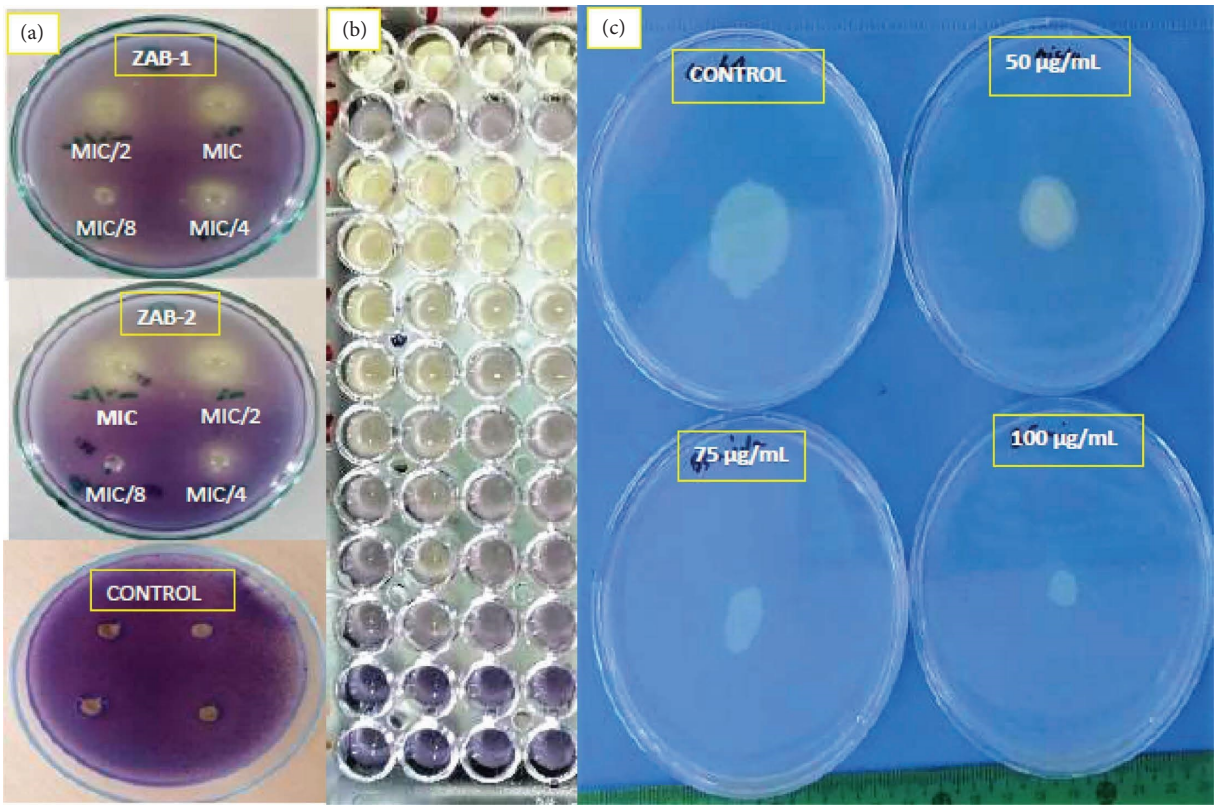

Figure 5: Quorum sensing inhibition plates against *C. violaceum* CV026 (a), violacein inhibition plates against *C. violaceum* CV12472 (b), and (c) swarming motility inhibition plates against *P. aeruginosa* PA01.

pigment caused by antimicrobial samples represents violacein inhibition, an anti-QS process [101]. QS systems inhibition is a strategy to block signal molecules like acylhomoserine lactone (AHL) from their biosynthesis or by degrading the AHL synthesized by the bacteria and/or inactivating receptor proteins for the produced AHL [91]. The synthesized hydrated zirconium oxide-alginate beads decreased the levels of violacein production, reflected in a decrease in violet coloration, as shown on Figure 5. The mutant strain *C. violaceum* CV026 equally failed to produce violacein within QS inhibition zones, as seen in Figure 5 as halos around the wells containing sample solutions at different concentrations.

Violacein inhibition assays with *C. violaceum* CV12472 indicated the potential inhibition of signal production while with *C. violaceum* CV026 indicated blockage of signal reception [6, 102–106]. The ability of the zirconium oxide-alginate beads to show antimicrobial activity, antibiofilm, and anti-QS potential on waterborne pathogens is a good indication that these materials can be suitable new biocides to treat infected water resources and avoid the development of resistant strains.

Table 5: Swarming motility inhibition on *P. aeruginosa* PA01 by test samples.

Sample codes	Swarming inhibition (%)		
	100 μg/mL	75 μg/mL	50 μg/mL
ZAB-1	25.1 ± 1.1	08.5 ± 0.2	—
ZAB-2	33.3 ± 1.2	17.5 ± 0.4	—

—: no inhibition.

3.4. Swarming Motility Inhibition against P. aeruginosa PA01. Substances that are able to inhibit virulence factors regulated by quorum sensing find applications as suitable therapies against infections and microbial resistance. Swarming motility is a virulence factor used by flagellated bacteria such as *P. aeruginosa* to move to nutrient-rich sites and targets. It also enables the bacteria to colonize surfaces and establish biofilms through the production of rhamnolipids on wet surfaces which facilitates swarming [107]. The flagellated *P. aeruginosa* PA01 was used in this assay and the diameters of growth (swarm diameters) on the plates were measured at 100 μg/mL, 75 μg/ml, and 50 μg/mL and used in calculating percentage inhibitions, and the results are presented in Table 5. Percentage inhibitions of swarming on *P. aeruginosa* PA01 were 25.1 ± 1.1% (ZAB-1) and 33.3 ± 1.2% (ZAB-2) at 100 μg/mL and 08.5 ± 0.2% (ZAB-1) and 17.5 ± 0.4% (ZAB-2) at 75 μg/mL and no inhibition of swarming was observed at 50 μg/mL. No significant difference was observed ($p > 0.05$) though the results indicated that ZAB-2 was slightly more active than ZAB-1. The zirconium oxide-alginate beads (ZAB-1 and ZAB-2) inhibited swarming motility in *P. aeruginosa* PA01, indicating that they can reduce the incidence of biofilms at an early stage and reduce the spread of bacteria. This is because bacteria use swarming motility to move towards nutrients and surfaces and then colonize the surfaces before forming biofilms [8, 108–111]. Swarming is facilitated by flagella and quorum sensing and usually involves the production of biosurfactants to reduce surface tension between bacteria cells and the surrounding environment and also pack them together in colonies [112]. Therefore, the inhibition of swarming and biofilms by the zirconium oxide-alginate beads can reduce biofouling in water. Polymeric materials are new types of antimicrobials with antivirulence effects on various pathogens and different modes of action, finding applications in multiple domains [113].

Purification technology plays a crucial role in the production of safe drinking water. The future prospects of this research will involve the development of safe biofilters from biodegradable polymers and metal oxides complexes which are endowed with antimicrobial effects. Biofiltration involves the purification of water using substances which can remove inorganic, organic pollutants, turbidity, undesirable tastes, and odours as well as bacteria and viruses. It is therefore interesting to develop biofilters with biodegradable polymers such as alginate which are compatible with the environment and can help address the increasing demand for drinking water. This technology is gaining attention because of its numerous advantages.

4. Conclusions

Access to colourless and odourless water that is free from contaminants and germs is a global problem. Portable water is necessary for basic life processes, and therefore all living organisms need water for their survival. The increasing population, rapid industrialization, and extensive agriculture lead to an increase in the contamination of available water resources. Many organic and inorganic chemical materials as well as some pathogenic microorganisms can get into water, and many techniques have been developed to effectively remove them while little attention is paid to the pathogenic bacteria that survive in water. This study reports the effects of synthesized hydrated zirconium metal oxide-coated alginate on some water-transmissible pathogenic bacteria. The hydrated zirconium oxide encapsulated in alginate biopolymer beads was synthesized and characterized by FT-IR, XRD, and SEM. They displayed antimicrobial, antibiofilm, and anti-QS properties on a range of waterborne bacteria. The anti-QS and antibiofilm effects indicated that the zirconium oxide-alginate material can prevent microbial resistance and biofouling of microbial communities in water. The addition of alginate is believed to render the particles more biocompatible and enables them to be easily recoverable from water after usage. The results therefore indicate the potential of treating water with zirconium oxide-alginate material as an environmentally friendly, nontoxic, and efficient strategy to inhibit waterborne microorganisms.

Data Availability

The data used to support the findings of this study are included within the article.

Conflicts of Interest

The authors declare that they have no conflicts of interest.

Acknowledgments

The authors are grateful to Mugla Sitki Kocman University, Turkey, University of Ngaoundere, Cameroon, and Dunarea de Jos University, Galati, Romania, for administrative and technical support as well as for the materials used in the experiments.

References

[1] S. Bidhuri, M. Taqi, and M. M. A. Khan, "Water-borne disease: link between human health and water use in the Mithepur and Jaitpur area of the NCT of Delhi," *Journal of Public Health*, vol. 26, no. 1, pp. 119–126, 2018.

[2] P. Kumar, S. Srivastava, A. Banerjee, and S. Banerjee, "Prevalence and predictors of water-borne diseases among elderly people in India: evidence from Longitudinal Ageing Study in India, 2017-18," *BMC Public Health*, vol. 22, no. 1, p. 993, 2022.

[3] F. Y. Ramírez-Castillo, A. Loera-Muro, M. Jacques et al., "Waterborne pathogens: detection methods and challenges," *Pathogens*, vol. 4, no. 2, pp. 307–334, 2015.

[4] J. K. Griffiths, *Waterborne Disease*, International Encyclopedia of Public Health, Academic Press, Cambridge, Massachusetts, USA, 2008.

[5] R. T. Pena, L. Blasco, A. Ambroa et al., "Relationship between quorum sensing and secretion systems," *Frontiers in Microbiology*, vol. 10, p. 1100, 2019.

[6] A. N. Tamfu, O. Ceylan, S. Kucukaydin, and M. E. Duru, "HPLC-DAD phenolic profiles, antibiofilm, anti-quorum sensing and enzyme inhibitory potentials of Camellia sinensis (L.) O. Kuntze and Curcuma longa L," *LWT--Food Science and Technology*, vol. 133, Article ID 110150, 2020.

[7] T. Alfred Ngenge, S. Kucukaydin, O. Ceylan, and M. E. Duru, "Evaluation of enzyme inhibition and anti-quorum sensing potentials of Melaleuca alternifolia and Citrus sinensis essential oils," *Natural Product Communications*, vol. 16, no. 9, pp. 1934578X2110445–8, 2021.

[8] X. Zhao, Z. Yu, and T. Ding, "Quorum-sensing regulation of antimicrobial resistance in bacteria," *Microorganisms*, vol. 8, no. 3, p. 425, 2020.

[9] A. N. Tamfu, O. Ceylan, G. C. Fru, M. Ozturk, M. E. Duru, and F. Shaheen, "Antibiofilm, antiquorum sensing and antioxidant activity of secondary metabolites from seeds of Annona senegalensis," *Persoon," Microbial Pathogenesis*, vol. 144, 2020.

[10] F. Opoku, E. M. Kiarii, P. P. Govender, and M. Mamo, "Metal oxide polymer nanocomposites in water treatments," in *Descriptive Inorganic Chemistry Researches of Metal Compounds*, IntechOpen, London, UK, 2017.

[11] B. Pan, B. Pan, W. L.-L. Zhang, L. Lv, Q. Zhang, and S. Zheng, "Development of polymeric and polymer-based hybrid adsorbents for pollutants removal from waters," *Chemical Engineering Journal*, vol. 151, no. 1-3, pp. 19–29, 2009.

[12] P. Alvarez, C. Blanco, and M. Granda, "The adsorption of chromium (VI) from industrial wastewater by acid and base-activated lignocellulosic residues," *Journal of Hazardous Materials*, vol. 144, no. 1-2, pp. 400–405, 2007.

[13] D. Shan, S. Deng, T. Zhao, G. Yu, J. Winglee, and M. R. Wiesner, "Preparation of regenerable granular carbon nanotubes by a simple heating-filtration method for efficient removal of typical pharmaceuticals," *Chemical Engineering Journal*, vol. 294, pp. 353–361, 2016.

[14] D. Liu, S. Deng, A. Maimaiti et al., "As (III) and as (V) adsorption on nanocomposite of hydrated zirconium oxide coated carbon nanotubes," *Journal of Colloid and Interface Science*, vol. 511, pp. 277–284, 2018.

[15] S. De Flora, "Threshold mechanisms and site specificity in chromium (VI) carcinogenesis," *Carcinogenesis*, vol. 21, no. 4, pp. 533–541, 2000.

[16] N. Daneshvar, D. Salari, and S. Aber, "Chromium adsorption and Cr (VI) reduction to trivalent chromium in aqueous solutions by soya cake," *Journal of Hazardous Materials*, vol. 94, no. 1, pp. 49–61, 2002.

[17] L. Khezami and R. Capart, "Removal of chromium (VI) from aqueous solution by activated carbons: kinetic and equilibrium studies," *Journal of Hazardous Materials*, vol. 123, no. 1-3, pp. 223–231, 2005.

[18] E. Katsou, S. Malamis, and K. J. Haralambous, "Industrial wastewater pre-treatment for heavy metal reduction by employing a sorbent-assisted ultrafiltration system," *Chemosphere*, vol. 82, no. 4, pp. 557–564, 2011.

[19] R. Kumar, S. J. Kim, K. H. Kim, S. H. Lee, H. S. Park, and B. H. Jeon, "Removal of hazardous hexavalent chromium from aqueous phase using zirconium oxide-immobilized alginate beads," *Applied Geochemistry*, vol. 88, pp. 113–121, 2018.

[20] A. Demir and M. Arisoy, "Biological and chemical removal of Cr (VI) from waste water: cost and benefit analysis," *Journal of Hazardous Materials*, vol. 147, no. 1-2, pp. 275–280, 2007.

[21] L. A. Rodrigues, L. J. Maschio, R. E. da Silva, and M. L. C. P. da Silva, "Adsorption of Cr (VI) from aqueous solution by hydrous zirconium oxide," *Journal of Hazardous Materials*, vol. 173, no. 1-3, pp. 630–636, 2010.

[22] T. M. Suzuki, J. O. Bomani, H. Matsunaga, and T. Yokoyama, "Preparation of porous resin loaded with crystalline hydrous zirconium oxide and its application to the removal of arsenic," *Reactive and Functional Polymers*, vol. 43, no. 1-2, pp. 165–172, 2000.

[23] A. Jain, V. Gupta, A. Bhatnagar, and S. Suhas, "A comparative study of adsorbents prepared from industrial wastes for removal of dyes," *Separation Science and Technology*, vol. 38, no. 2, pp. 463–481, 2003.

[24] V. K. Gupta, S. Agarwal, and T. A. Saleh, "Synthesis and characterization of alumina-coated carbon nanotubes and their application for lead removal," *Journal of Hazardous Materials*, vol. 185, no. 1, pp. 17–23, 2011.

[25] V. K. Gupta, A. Mittal, D. Jhare, and J. Mittal, "Batch and bulk removal of hazardous colouring agent Rose Bengal by adsorption techniques using bottom ash as adsorbent," *RSC Advances*, vol. 2, no. 22, pp. 8381–8389, 2012.

[26] V. K. Gupta, R. Kumar, A. Nayak, T. A. Saleh, and M. Barakat, "Adsorptive removal of dyes from aqueous solution onto carbon nanotubes: a review," *Advances in Colloid and Interface Science*, vol. 193, pp. 24–34, 2013.

[27] X. Luo, C. Wang, L. Wang et al., "Nanocomposites of graphene oxide-hydrated zirconium oxide for simultaneous removal of As(III) and As(V) from water," *Chemical Engineering Journal*, vol. 220, pp. 98–106, 2013.

[28] D. W. Cho, W. Jung, A. Sigdel et al., "Adsorption of Pb (II) and Ni (II) from aqueous solution by nanosized graphite carbon-impregnated calcium alginate bead," *Geosystem Engineering*, vol. 16, no. 3, pp. 200–208, 2013.

[29] D. Balarak, J. Jaafari, G. Hassani et al., "The use of low-cost adsorbent (Canola residues) for the adsorption of methylene blue from aqueous solution: isotherm, kinetic and thermodynamic studies," *Colloids and Interface Science Communications*, vol. 7, pp. 16–19, 2015.

[30] D.-W. Cho, B.-H. Jeon, Y. Jeong et al., "Synthesis of hydrous zirconium oxide-impregnated chitosan beads and their application for removal of fluoride and lead," *Applied Surface Science*, vol. 372, pp. 13–19, 2016.

[31] B. Chen, Z. Zhu, S. Liu et al., "Facile hydrothermal synthesis of nanostructured hollow iron – cerium alkoxides and their superior arsenic adsorption performance," *ACS Applied Materials and Interfaces*, vol. 6, no. 16, pp. 14016–14025, 2014.

[32] L. Hao, T. Zheng, J. Jiang, G. Zhang, and P. Wang, "Removal of as (III) and as (V) from water using iron doped amino functionalized sawdust: characterization, adsorptive performance and UF membrane separation," *Chemical Engineering Journal*, vol. 292, pp. 163–173, 2016.

[33] B. Peng, T. Song, T. Wang et al., "Facile synthesis of Fe_3O_4@ $Cu(OH)_2$ composites and their arsenic adsorption application" Chemical Engineering," *Chemical Engineering Journal*, vol. 299, pp. 15–22, 2016.

[34] J. Mertens, J. Rose, B. Wehrli, and G. Furrer, "Arsenate uptake by Al nanoclusters and other Al based sorbents

during water treatment," *Water Research*, vol. 88, pp. 844–851, 2016.

[35] J. Ju, R. Liu, Z. He, H. Liu, X. Zhang, and J. Qu, "Utilization of aluminum hydroxide waste generated in fluoride adsorption and coagulation processes for adsorptive removal of cadmium ion," *Frontiers of Environmental Science and Engineering*, vol. 10, no. 3, pp. 467–476, 2016.

[36] D. Ocinski, I. Jacukowicz-Sobala, P. Mazur, J. Raczyk, and E. Kociołek-Balawejder, "Water treatment residuals containing iron and manganese oxides for arsenic removal from water – characterization of physicochemical properties and adsorption studies," *Chemical Engineering Journal*, vol. 294, pp. 210–221, 2016.

[37] M. L. Peralta Ramos, J. A. González, S. G. Albornoz et al., "Chitin hydrogel reinforced with TiO_2 nanoparticles as an arsenic sorbent," *Chemical Engineering Journal*, vol. 285, pp. 581–587, 2016.

[38] T. Mwamulima, X. Zhang, Y. Wang, S. Song, and C. Peng, "Novel approach to control adsorbent aggregation: iron fixed bentonite-fly ash for Lead (Pb) and Cadmium (Cd) removal from aqueous media," *Frontiers of Environmental Science and Engineering*, vol. 12, no. 2, p. 2, 2018.

[39] B. K. Biswas, J.-I. Inoue, K. Inoue et al., "Adsorptive removal of as (V) and as (III) from water by a Zr (IV)-loaded orange waste gel," *Journal of Hazardous Materials*, vol. 154, no. 1-3, pp. 1066–1074, 2008.

[40] S. Mandal, T. Padhi, and R. Patel, "Studies on the removal of arsenic (III) from water by a novel hybrid material," *Journal of Hazardous Materials*, vol. 192, no. 2, pp. 899–908, 2011.

[41] H. Cui, Q. Li, S. Gao, and J. K. Shang, "Strong adsorption of arsenic species by amorphous zirconium oxide nanoparticles," *Journal of Industrial and Engineering Chemistry*, vol. 18, no. 4, pp. 1418–1427, 2012.

[42] W. Xu, J. Wang, L. Wang et al., "Enhanced arsenic removal from water by hierarchically porous CeO2–ZrO2 nanospheres: role of surface-and structure-dependent properties," *Journal of Hazardous Materials*, vol. 260, pp. 498–507, 2013.

[43] H. Cui, Y. Su, Q. Li, S. Gao, and J. K. Shang, "Exceptional arsenic (III, V) removal performance of highly porous, nanostructured ZrO2 spheres for fixed bed reactors and the full-scale system modeling," *Water Research*, vol. 47, no. 16, pp. 6258–6268, 2013.

[44] S. F. Lim, Y. M. Zheng, S. W. Zou, and J. P. Chen, "Characterization of copper adsorption onto an alginate encapsulated magnetic sorbent by a combined FT-IR, XPS, and mathematical modeling study," *Environmental Science and Technology*, vol. 42, no. 7, pp. 2551–2556, 2008.

[45] M. A. Khan, W. Jung, O. H. Kwon et al., "Sorption studies of manganese and cobalt from aqueous phase onto alginate beads and nano-graphite encapsulated alginate beads," *Journal of Industrial and Engineering Chemistry*, vol. 20, no. 6, pp. 4353–4362, 2014.

[46] O. H. Kwon, J. O. Kim, D. W. Cho et al., "Adsorption of as (III), as (V) and Cu (II) on zirconium oxide immobilized alginate beads in aqueous phase," *Chemosphere*, vol. 160, pp. 126–133, 2016.

[47] V. M. Boddu, K. Abburi, J. L. Talbott, E. D. Smith, and R. Haasch, "Removal of arsenic (III) and arsenic (V) from aqueous medium using chitosan-coated biosorbent," *Water Research*, vol. 42, no. 3, pp. 633–642, 2008.

[48] S. M. Miller, M. L. Spaulding, and J. B. Zimmerman, "Optimization of capacity and kinetics for a novel bio-based arsenic sorbent, TiO2-impregnated chitosan bead," *Water Research*, vol. 45, no. 17, pp. 5745–5754, 2011.

[49] B. Pan, Z. Li, Y. Zhang et al., "Acid and organic resistant nano-hydrated zirconium oxide (HZO)/polystyrene hybrid adsorbent for arsenic removal from water," *Chemical Engineering Journal*, vol. 248, pp. 290–296, 2014.

[50] P. Sivagurunathan, G. Kumar, and C. Y. Lin, "Hydrogen and ethanol fermentation of various carbon sources by immobilized Escherichia coli (XL1-Blue)," *International Journal of Hydrogen Energy*, vol. 39, no. 13, pp. 6881–6888, 2014.

[51] G. Kumar, P. Sivagurunathan, J. H. Park, and S. H. Kim, "Improved hydrogen production from galactose via immobilized mixed consortia," *Arabian Journal for Science and Engineering*, vol. 40, no. 8, pp. 2117–2122, 2015.

[52] G. S. Anisha and P. Prema, "Cell immobilization technique for the enhanced production of α-galactosidase by Streptomyces griseoloalbus," *Bioresource Technology*, vol. 99, no. 9, pp. 3325–3330, 2008.

[53] H. Liu, K. Zuo, and C. D. Vecitis, "Titanium dioxide-coated carbon nanotube network filter for rapid and effective arsenic sorption," *Environmental Science and Technology*, vol. 48, no. 23, pp. 13871–13879, 2014.

[54] J. C. Debsikdar, "Transparent zirconia gel-monolith from zirconium alkoxide," *Journal of Non-crystalline Solids*, vol. 86, no. 1-2, pp. 231–240, 1986.

[55] A. Mondal and S. Ram, "Monolithic t-ZrO_2 nano-powder through a $ZrO(OH)_2$ xH_2O polymer precursor," *Journal of the American Ceramic Society*, vol. 87, no. 12, pp. 2187–2194, 2004.

[56] M. D. M. Lleò, C. Signoretto, and P. Canepar, "Gram-positive bacteria in the marine environment," in *Oceans and Health: Pathogens in the Marine Environment*, S. Belkin and R. R. Colwell, Eds., Springer, Boston, MA, USA, 2005.

[57] H. C. Steffen, K. Smith, C. van Deventer et al., "Health risk posed by direct ingestion of yeasts from polluted river water," *Water Research*, vol. 231, no. 231, Article ID 119599, 2023.

[58] B. Alisjahbana, J. Debora, E. Susandi, and G. Darmawan, "Chromobacterium violaceum: a review of an unexpected scourge," *International Journal of General Medicine*, vol. 14, pp. 3259–3270, 2021.

[59] A. N. Tamfu, A. M. Munvera, A. V. D. Botezatu et al., "Synthesis of benzoyl esters of β-amyrin and lupeol and evaluation of their antibiofilm and antidiabetic activities," *Results in Chemistry*, vol. 4, 2022.

[60] J. H. Merritt, D. E. Kadouri, and G. A. O'Toole, "Growing and analyzing static biofilms," *Current Protocols in Microbiol*, John Wiley and Sons, Inc, Hoboken, NJ, USA, 2005.

[61] A. N. Tamfu, O. Ceylan, S. Kucukaydin, M. Ozturk, M. E. Duru, and R. M. Dinica, "Antibiofilm and enzyme inhibitory potentials of two Annonaceous food spices, African pepper (Xylopia aethiopica) and African nutmeg (Monodora myristica)," *Foods*, vol. 9, no. 12, p. 1768, 2020.

[62] K. H. Koh and F. Y. Tham, "Screening of traditional Chinese medicinal plants for quorum-sensing inhibitors activity," *Journal of Microbiology, Immunology, and Infection*, vol. 44, no. 2, pp. 144–148, 2011.

[63] G. Kocak, A. N. Tamfu, V. Bütün, and O. Ceylan, "Synthesis of quaternary piperazine methacrylate homopolymers and their antibiofilm and anti-quorum sensing effects on pathogenic bacteria," *Journal of Applied Polymer Science*, vol. 138, no. 21, 2021.

[64] H. Beddiar, S. Boudiba, M. Benahmed et al., "Chemical composition, anti-quorum sensing, enzyme inhibitory, and antioxidant properties of phenolic extracts of Clinopodium nepeta," *Plants*, vol. 10, no. 9, p. 1955, 2021.

[65] S. Boudiba, A. N. Tamfu, B. Berka et al., "Anti-quorum sensing and antioxidant activity of essential oils extracted from Juniperus species, growing spontaneously in Tebessa Region (East of Algeria)," *Natural Product Communications*, vol. 16, no. 6, pp. 1934578X2110240–11, 2021.

[66] I. A. Sybiya Vasantha Packiavathy, P. Agilandeswari, K. S. Musthafa, S. Karutha Pandian, and A. Veera Ravi, "Antibiofilm and quorum sensing inhibitory potential of *Cuminum cyminum* and its secondary metabolite methyl eugenol against Gram negative bacterial pathogens," *Food Research International*, vol. 45, no. 1, pp. 85–92, 2012.

[67] A. N. Tamfu, S. Kucukaydin, M. M. Quradha, O. Ceylan, A. Ugur, and M. E. Duru, "Ultrasound-assisted extraction of Syringa vulgaris Mill., Citrus sinensis L. and Hypericum perforatum L.: phenolic composition, enzyme inhibition and anti-quorum sensing activities," *Chemistry Africa*, vol. 5, no. 2, pp. 237–249, 2022.

[68] S. Zinatloo-Ajabshir and M. Salavati-Niasari, "Synthesis of pure nanocrystalline ZrO_2 via a simple sonochemical-assisted route," *Journal of Industrial and Engineering Chemistry*, vol. 20, no. 5, pp. 3313–3319, 2014.

[69] F. Heshmatpour and R. B. Aghakhanpour, "Synthesis and characterization of nanocrystalline zirconia powder by simple sol–gel method with glucose and fructose as organic additives," *Powder Technology*, vol. 205, no. 1-3, pp. 193–200, 2011.

[70] Y. İspirli Doğaç and M. Teke, "Urease immobilized core–shell magnetic Fe [NiFe] O_4/alginate and Fe_3O_4/alginate composite beads with improved enzymatic stability properties: removal of artificial blood serum urea," *Journal of the Iranian Chemical Society*, vol. 18, no. 10, pp. 2637–2648, 2021.

[71] L. Kumari, W. Z. Li, J. M. Xu et al., "Controlled hydrothermal synthesis of zirconium oxide nanostructures and their optical properties," *Crystal Growth and Design*, vol. 9, pp. 3874–3880, 2009.

[72] J. Luo, X. Luo, J. Crittenden et al., "Removal of antimonite (Sb(III)) and antimonate (Sb(V)) from aqueous solution using carbon nanofibers that are decorated with zirconium oxide (ZrO_2)," *Environmental Science and Technology*, vol. 49, no. 18, pp. 11115–11124, 2015.

[73] M. Jafarpour, E. Rezapour, M. Ghahramaninezhad, and A. Rezaeifard, "A novel protocol for selective synthesis of monoclinic zirconia nanoparticles as a heterogeneous catalyst for condensation of 1,2-diamines with 1,2-dicarbonyl compounds," *New Journal of Chemistry*, vol. 38, no. 2, pp. 676–682, 2014.

[74] E. Hemalatha and N. Gopalakrishnan, "Synthesis of ZrO_2 nanostructure for gas sensing application," *Bulletin of Materials Science*, vol. 43, no. 1, p. 12, 2020.

[75] M. N. Chu, M. X. Truong, T. H. L. Nguyen et al., "Purification and characterization of high purity nano zirconia by liquid-liquid extraction using d2ehpa/p-xylenes," *Inorga*, vol. 10, no. 7, p. 93, 2022.

[76] S. Mallakpour and F.-S. Sadeghi-Kaji, "Hydrogel bionanocomposite beads based on alginate and silica: physicochemical and in vitro bioactivity evaluations," *Polymer Bulletin*, vol. 80, no. 8, pp. 9097–9111, 2022.

[77] S. Stojadinovic, R. Vasilic, N. Radic, and B. Grbic, "Zirconia films formed by plasma electrolytic oxidation: photoluminescent and photocatalytic properties," *Optical Materials*, vol. 40, pp. 20–25, 2015.

[78] H. Sharifi, M. Divandari, A. Khavandi, and M. H. Idris, "Effect of Al powder and silica sol on the structure and mechanical properties of Al_2O_3-ZrO_2 foams," *Acta Metallurgica Sinica*, vol. 23, pp. 241–247, 2010.

[79] F. Gonell, D. Portehault, B. Julián-López, K. Vallé, C. Sanchez, and A. Corma, "One step microwave-assisted synthesis of nanocrystalline WOx–ZrO_2 acid catalysts," *Catalysis Science and Technology*, vol. 6, no. 23, pp. 8257–8267, 2016.

[80] S. Plumejeau, J. G. Alauzun, and B. Boury, "Hybrid metal oxide@biopolymer materials precursors of metal oxides and metal oxide-carbon composites," *Journal of the Ceramic Society of Japan*, vol. 123, no. 1441, pp. 695–708, 2015.

[81] O. Ceylan, A. N. Tamfu, Y. İ. Doğaç, and M. Teke, "Antibiofilm and anti-quorum sensing activities of polyethylene imine coated magnetite and nickel ferrite nanoparticles," *3 Biotech*, vol. 10, no. 12, p. 513, 2020.

[82] S. Sarkar, E. Guibal, F. Quignard, and A. K. SenGupta, "Polymer-supported metals and metal oxide nanoparticles: synthesis, characterization, and applications," *Journal of Nanoparticle Research*, vol. 14, no. 2, p. 715, 2012.

[83] E. Weidner, E. Karbassiyazdi, A. Altaee, T. Jesionowski, and F. Ciesielczyk, "Hybrid metal oxide/biochar materials for wastewater treatment technology: a review," *ACS Omega*, vol. 7, no. 31, pp. 27062–27078, 2022.

[84] A. Moghaddam, R. Ranjbar, M. Yazdanian et al., "The current antimicrobial and antibiofilm activities of synthetic/herbal/biomaterials in dental application," *BioMed Research International*, vol. 2022, Article ID 8856025, 26 pages, 2022.

[85] T. Naseem and T. Durrani, "The role of some important metal oxide nanoparticles for wastewater and antibacterial applications: a review," *Environmental Chemistry and Ecotoxicology*, vol. 3, pp. 59–75, 2021.

[86] X. Chen and S. S. Mao, "Titanium dioxide nanomaterials: synthesis, properties, modifications, and applications," *ChemInform*, vol. 38, no. 41, pp. 2891–2959, 2007.

[87] P. Joshi, K. Gupta, R. Gusain, and O. P. Khatri, *Metal Oxide Nanocomposites for Wastewater Treatment, Metal Oxide Nanocomposites: Synthesis and Applications*, Scrivener Publishing LLC, Beverly, MA, USA, 2020.

[88] N. Tahir, M. Zahid, I. A. Bhatti, A. Mansha, S. A. R. Naqvi, and T. Hussain, "Metal oxide-based ternary nanocomposites for wastewater treatment," *Aquananotechnology*, vol. 2021, pp. 135–158, 2021.

[89] P. Joshi, A. Raturi, M. Srivastava, and O. P. Khatri, "Graphene oxide, kaolinite clay and PVA-derived nanocomposite aerogel as a regenerative adsorbent for wastewater treatment applications," *Journal of Environmental Chemical Engineering*, vol. 10, no. 6, Article ID 108597, 2022.

[90] P. Jain and T. Pradeep, "Potential of silver nanoparticle-coated polyurethane foam as an antibacterial water filter," *Biotechnology and Bioengineering*, vol. 90, no. 1, pp. 59–63, 2005.

[91] M. Asadpoor, G. N. Ithakisiou, J. P. M. van Putten, R. J. Pieters, G. Folkerts, and S. Braber, "Antimicrobial activities of alginate and chitosan oligosaccharides against Staphylococcus aureus and Group B Streptococcus," *Frontiers in Microbiology*, vol. 13, 2021.

[92] M. Bustamante-Torres, B. Arcentales-Vera, J. Estrella-Nuñez, H. Yánez-Vega, and E. Bucio, "Antimicrobial activity of composites-based on biopolymers," *Macromolecules (Washington, DC, United States)*, vol. 2, no. 3, pp. 258–283, 2022.

[93] H. S. Vasavi, A. B. Arun, and P. D. Rekha, "Inhibition of quorum sensing in Chromobacterium violaceum by

Syzygium cumini L. and *Pimenta dioica* L," *Asian Pacific Journal of Tropical Biomedicine*, vol. 3, no. 12, pp. 954–959, 2013.

[94] K. H. McClean, M. K. Winson, L. Fish et al., "Quorum sensing and Chromobacterium violaceum: exploitation of violacein production and inhibition for the detection of N-acylhomoserine lactones," *Microbiology (Reading)*, vol. 143, no. 12, pp. 3703–3711, 1997.

[95] A. N. Tamfu, S. Kucukaydin, O. Ceylan, N. Sarac, and M. E. Duru, "Phenolic composition, enzyme inhibitory and anti-quorum sensing activities of cinnamon (Cinnamomum zeylanicum Blume) and Basil (Ocimum basilicum Linn)," *Chemistry Africa*, vol. 4, no. 4, pp. 759–767, 2021.

[96] B. Sun, H. Luo, H. Jiang, Z. Wang, and A. Jia, "Inhibition of quorum sensing and biofilm formation of esculetin on Aeromonas hydrophila," *Frontiers in Microbiology*, vol. 12, Article ID 737626, 2021.

[97] A. N. Tamfu, O. Ceylan, G. Cârâc, E. Talla, and R. M. Dinica, "Antibiofilm and anti-quorum sensing potential of cycloartane-type triterpene acids from Cameroonian grassland propolis: phenolic profile and antioxidant activity of crude extract," *Molecules*, vol. 15, 2022.

[98] G. N. McAuliffe, R. W. Baird, and J. Hennessy, "Relative frequency, characteristics and antimicrobial susceptibility patterns of *Vibrio spp., Aeromonas spp.,* Chromobacterium violaceum, and Shewanella spp. in the Northern territory of Australia, 2000–2013," *The American Journal of Tropical Medicine and Hygiene*, vol. 92, no. 3, pp. 605–610, 2015.

[99] Y. D. Lin, J. Hennessy, S. S. Majumdar, and R. W. Baird, "The Spectrum of Chromobacterium violaceum infections from a single geographic location," *The American Journal of Tropical Medicine and Hygiene*, vol. 94, no. 4, pp. 710–716, 2016.

[100] A. Ngenge, O. Ceylan, G. Fru, Y. Arab, D. Emin, and M. Ozturk, "Antimicrobial, antibiofilm, anti-quorum sensing and motility inhibition activities of essential oil from seeds of food spice Xylopia aethiopica (Dunal) A. Rich. on some pathogenic bacteria," *Research Journal of Biotechnology*, vol. 16, pp. 68–76, 2021.

[101] T. N. Alfred, O. Ceylan, S. Kucukaydin et al., "HPLC-DAD and GC-MS characterization of Cameroonian honey samples and evaluation of their antibiofilm, anti-quorum sensing and antioxidant activities," *Bulletin of Environment, Pharmacology and Life Science*, vol. 9, no. 10, pp. 132–142, 2020.

[102] R. Belapurkar, V. S. Tale, and R. Madkaikar, "Exploiting quorum sensing to inhibit the bacterial pathogens," *International Journal of Current Microbiology and Applied Science*, vol. 3, pp. 453–458, 2014.

[103] M. Popova, D. Gerginova, B. Trusheva et al., "A preliminary study of chemical profiles of honey, cerumen, and propolis of the African stingless bee Meliponula ferruginea," *Foods*, vol. 10, no. 5, p. 997, 2021.

[104] A. Ngenge Tamfu, W. Boukhedena, S. Boudiba, S. Deghboudj, and O. Ceylan, "Synthesis and evaluation of inhibitory potentials of microbial biofilms and quorum-sensing by 3-(1, 3-dithian-2-ylidene) pentane-2, 4-dione and ethyl-2-cyano-2-(1, 3-dithian-2-ylidene) acetate," *Pharmacia*, vol. 69, no. 4, pp. 973–980, 2022.

[105] S. Boudiba, A. N. Tamfu, K. Hanini et al., "Synthesis of a new diarylhydrazone derivative and an evaluation of its in vitro biofilm inhibition and quorum sensing disruption along with a molecular docking study," *Journal of Chemical Research*, vol. 47, no. 4, 2023.

[106] H. N. Ikome, A. N. Tamfu, J. P. Abdou et al., "Disruption of biofilm formation and quorum sensing in pathogenic bacteria by compounds from zanthoxylum gilletti (de wild) PG waterman," *Applied Biochemistry and Biotechnology*, vol. 195, no. 10, pp. 6113–6131, 2023.

[107] D. Lakshmanan, J. Nanda, and K. Jeevaratnam, "Inhibition of swarming motility of *Pseudomonas aeruginosa* by methanol extracts of Alpinia officinarum Hance. and *Cinnamomum tamala* T. Nees and Eberm," *Natural Product Research*, vol. 32, no. 11, pp. 1307–1311, 2018.

[108] K. Y. Alain, A. N. Tamfu, S. Kucukaydin et al., "Phenolic profiles, antioxidant, antiquorum sensing, antibiofilm and enzyme inhibitory activities of selected Acacia species collected from Benin," *Lebensmittel-Wissenschaft und-Technologie*, vol. 12, 2022.

[109] Y. Arab, B. Sahin, O. Ceylan et al., "Assessment of in vitro activities and chemical profiling of Senecio hoggariensis growing in Algerian Sahara," *Biodiversitas*, vol. 23, no. 7, pp. 3498–3506, 2022.

[110] I. Grobas, D. G. Bazzoli, and M. Asally, "Biofilm and swarming emergent behaviours controlled through the aid of biophysical understanding and tools," *Biochemical Society Transactions*, vol. 48, no. 6, pp. 2903–2913, 2020.

[111] L. Hou, A. Debru, Q. Chen, Q. Bao, and K. Li, "AmrZ regulates swarming motility through cyclic di-GMP-dependent motility inhibition and controlling pel polysaccharide production in Pseudomonas aeruginosa PA14," *Frontiers in Microbiology*, vol. 10, p. 1847, 2019.

[112] R. M. Talla, A. N. Tamfu, B. N. Wakeu et al., "Evaluation of anti-quorum sensing and antibiofilm effects of secondary metabolites from Gambeya lacourtiana (De Wild) Aubr. and Pellegr against selected pathogens," *BMC Complementary Medicine and Therapies*, vol. 23, no. 1, pp. 300–306, 2023.

[113] A. N. Tamfu, G. Kocak, O. Ceylan, F. Valentine, V. Bütün, and H. Çiçek, "Synthesis of cross-linked diazaborine-based polymeric microparticles with antiquorum sensing, anti-swarming, antimicrobial, and antibiofilm properties," *Journal of Applied Polymer Science*, vol. 140, no. 11, 2023.